Modeling, Calibration, and Correction of Nonlinear Illumination-Dependent Fixed Pattern Noise in Logarithmic CMOS Image Sensors

Dileepan Joseph and Steve Collins

***Abstract*—At present, most CMOS image sensors use an array of pixels with a linear response. However, pixels with a logarithmic response are also possible and are capable of imaging high dynamic range scenes without saturating. Unfortunately, logarithmic image sensors suffer from fixed pattern noise (FPN). Work reported in the literature generally assumes the FPN is independent of illumination. This paper develops a nonlinear model $y = a + b\ln(c + x) + \epsilon$ of a pixel for the digital response y to an illuminance x and shows that the FPN arises from a variation of the offset a, gain b, and bias c from pixel to pixel. Equations are derived to estimate these parameters by calibrating images of uniform stimuli, taken with varying illuminances. Experiments with a Fuga 15d image sensor, demonstrating parameter calibration and FPN correction, show that the nonlinear model outperforms previous models that assume either only offset or offset and gain variation.**

***Index Terms*—CMOS image sensors, fixed pattern noise, logarithmic pixels.**

I. Introduction

THE CCD image sensor, a dominant technology for nearly three decades, faces tough competition from the CMOS image sensor [1]–[3], a more recent technology. Since their fabrication process is incompatible with conventional electronics, CCD sensors require external circuits to provide bias voltages, clock signals, control logic, analog-to-digital conversion and signal processing. CMOS technology, however, permits the integration of these circuits on the same die as the sensor to reduce the cost, power consumption, size and weight of the final camera. Fundamentally, CMOS pixels scale well with shrinking process geometries because more electronics can be placed in each pixel to improve the output without affecting sensitivity or resolution. For these and other reasons, such as a higher quantum efficiency, less smear and blooming, better yields and price pressure from more competition, the electronics industry expects CMOS gradually to replace CCD image sensors.

This paper concerns a subset of CMOS sensor technology, namely logarithmic imagers. Unlike a linear pixel (CCD or CMOS), which integrates the charge produced by photon absorption over a finite period, a logarithmic pixel, as in Fig. 1, continuously converts incident photons into a voltage that is proportional to the logarithm of the light intensity over more than five decades of illuminance [4]. Such a nonintegrating sensor can be randomly accessed in space and time, a feature useful in some industrial applications for which frame size and speed may be traded against each other. As these pixels are simple, consisting of three transistors and a diode, sensors have been made with 2048 x 2048 pixels and acceptable yields [5].

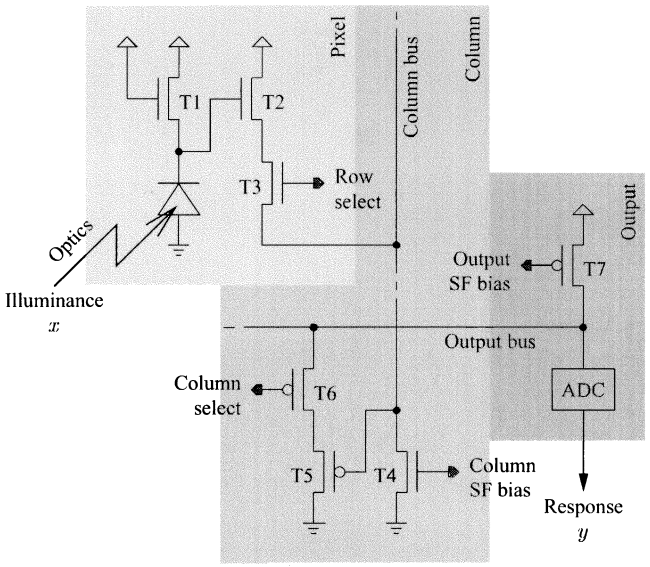

Fig. 1. From an illuminance x to a digital response y in one pixel of a logarithmic CMOS image sensor. T2 with T4 and T5 with T7 form an NMOS and PMOS source follower (SF), respectively, when T3 and T6 are turned on.

In reality, light reflected by scenes spans many decades of illuminance, from 0.001 lux at night to between 1 and 1000 lux in indoor lighting and up to 10 000 lux in bright sunlight [6]. Direct viewing and specularities of bright sources, such as oncoming headlights or the sun, may lead to higher intensities. The advantage of a logarithmic sensor is that, over five decades of illuminance, ten bits of resolution are sufficient to sense illuminance with one percent accuracy. With a linear sensor, 23 bits are necessary to accomplish the same task. This would be costly for still cameras and extremely difficult at video rates. Of course, a linear sensor with a smaller resolution could adapt over a large dynamic range by aperture or integration-time control. However, saturated patches (black or white) would appear in images of scenes that span a high dynamic range, such as most outdoor scenes in daylight or an indoor scene with a bright window. Many nonlogarithmic methods have been proposed to extend the dynamic range of image sensors [6], but most result in decreased resolution, sensitivity or frame rate.

Manuscript received May 29, 2001; revised August 11, 2002.

The authors are with the Department of Engineering Science, University of Oxford, Oxford, U.K. (e-mail: dileepan@robots.ox.ac.uk; collins@robots.ox.ac.uk).

Digital Object Identifier 10.1109/TIM.2002.807803

One disadvantage of a logarithmic sensor is a loss of the averaging effect of integration, which improves low-light sensitivity [4]. However, the biggest problem by far is fixed pattern noise (FPN), which is a distortion of the image due to variations in device parameters across the sensor. Dierickx, Scheffer, Loose, and others have developed digital and analog methods to correct this error by assuming it is independent of illuminance [4], [5], [7]. Loose *et al.* briefly considered FPN as a linear function of illuminance, but they were unable to compensate for this dependence with their analog circuit architecture and concluded that it was not significant [7]. However, Yadid-Pecht notes that FPN varies nonlinearly with illuminance in a logarithmic sensor, but she neither characterizes nor attempts to correct this distortion [6], which is the subject of this paper. Section II models the response of a logarithmic pixel to illuminance. Section III derives equations to calibrate the model, from images of a uniform scene, and to correct FPN. Section IV gives experimental results of calibration and correction.

II. Modeling

Fig. 1 shows the process by which the light stimulus, of illuminance x, falling on a pixel in a typical logarithmic CMOS sensor is converted to a digital response y. Before the light reaches the photodiode in the pixel, it is attenuated due to absorption and reflection by the aperture and lens of the camera, which may be represented by gains G_A and G_L. Photons absorbed by the photodiode form electron-hole pairs that are swept out by the electric field across the device to produce a current I_P, given in (1). This photocurrent is linearly related to the incident light intensity over many orders of magnitude. The relationship depends on the quantum efficiency, which may be represented by a gain G_Q and the light-sensitive area A of the photodiode:

$$I_P = G_A G_L G_Q A x. \tag{1}$$

The photodiode in Fig. 1 is reverse biased to prevent any current flowing to ground through it except for the photocurrent. However, a small leakage current I_S, known as the reverse bias saturation current, also flows to ground through this diode. The total current $I_P + I_S$ sets the gate voltage V_G^{T2}, given in (2) where V_{DD} is the supply voltage, of transistor T2 via the diode-connected load transistor T1. Designed to operate in the subthreshold region, T1 has a logarithmic current-to-voltage relationship that is valid over many decades of current amplitude:

$$V_G^{\mathrm{T2}} = V_{DD} - \frac{n^{\mathrm{T1}} kT}{q} \ln\left(\frac{I_p + I_s}{I_{on}^{\mathrm{T1}}}\right) - V_{on}^{\mathrm{T1}}. \tag{2}$$

Transistor T3 is a switch that is either an open or a short circuit between T2 and the common bus for a column of pixels. This column bus is biased by transistor T4. When T3 is off, T2 is disconnected from the bus and does not affect its voltage. When T3 is on, a similar switch is off for all other pixels in the column and the gate voltage V_G^{T5} of transistor T5, given in (3), equals the source voltage V_S^{T2} of T2. As T2 and T4 have the same drain-source current, when T3 is on and as both operate in saturation, their gate-source minus threshold voltages $V_{GS}^{\mathrm{T2}} - V_T^{\mathrm{T2}}$ and $V_{GS}^{\mathrm{T4}} - V_T^{\mathrm{T4}}$ are linearly related:

$$V_G^{\mathrm{T5}} = V_G^{\mathrm{T2}} - V_T^{\mathrm{T2}} - \sqrt{\frac{K^{\mathrm{T4}}}{K^{\mathrm{T2}}}}\left(V_{GS}^{\mathrm{T4}} - V_T^{\mathrm{T4}}\right). \tag{3}$$

When a pixel is connected to the bus for its column, all pixels in the same row are connected to their respective column buses. However, the analog-to-digital converter (ADC) processes only one voltage at a time. Therefore, the column buses are switched in sequence onto a common output bus, which is biased by transistor T7, using a two-transistor circuit similar to the one described above. When transistor T6 is switched on, T5 is connected to the output bus and the voltage V_{ADC} at the input of the ADC, given in (4), equals the source voltage V_S^{T5} of T5:

$$V_{ADC} = V_G^{\mathrm{T5}} - V_T^{\mathrm{T5}} - \sqrt{\frac{K^{\mathrm{T7}}}{K^{\mathrm{T5}}}}\left(V_{GS}^{\mathrm{T7}} - V_T^{\mathrm{T7}}\right) \tag{4}$$

Rather than getting into the details of ADC circuits, (5) abstracts the digitization of voltage V_{ADC} by a clipping function, to limit the maximum and minimum output values and by rounding off, which introduces quantization error. Furthermore, the ADC adjusts its input V_{ADC} by an offset F_{ADC} and gain G_{ADC} to fit the domain of voltages to the range of integer codes (e.g., 0–255 LSB for an 8-bit ADC):

$$y = \mathrm{round}\left(\mathrm{clip}\left(F_{ADC} + G_{ADC} V_{ADC}\right)\right). \tag{5}$$

If the input voltage does not cause clipping, digitization may be modeled by a quantization error term ϵ_Q, with a range of ± 0.5 LSB, that is added to the output. Furthermore, the whole process in Fig. 1 will add noise components at various stages. However, the noise shall be modeled by a single random variable ϵ_N added to the output. A further term ϵ_D may be added to the output to account for error in the underlying device equations. Considering these remarks, (6) gives the digital response y of a pixel:

$$y = F_{ADC} + G_{ADC} V_{ADC} + \epsilon_Q + \epsilon_N + \epsilon_D. \tag{6}$$

Grouping the equations and physical parameters above, (7)–(11) give the digital response y of a pixel as a logarithm of the illuminance x, with three abstract parameters a, b, and c, named the *offset*, *gain*, and *bias*, and a residual error ϵ. A variation from pixel to pixel of a, b, c, or a combination thereof, causes FPN. Therefore, these parameters must be estimated by calibration to correct FPN in an image. Furthermore, the statistics of the output-referred error ϵ (the error may also be referred to the input x) must be estimated to validate the model and determine the accuracy of calibration and correction:

$$y = a + b\ln(c + x) + \epsilon \tag{7}$$

$$\begin{aligned} a = {} & F_{ADC} + G_{ADC} \\ & \cdot \left(V_{DD} + \frac{n^{\mathrm{T1}} kT}{q} \ln\left(\frac{I_{on}^{\mathrm{T1}}}{G_A G_L G_Q A}\right) \right. \\ & - V_{on}^{\mathrm{T1}} - V_T^{\mathrm{T2}} - \sqrt{\frac{K^{\mathrm{T4}}}{K^{\mathrm{T2}}}}\left(V_{GS}^{\mathrm{T4}} - V_T^{\mathrm{T4}}\right) \Big) \\ & \left. - V_T^{\mathrm{T5}} - \sqrt{\frac{K^{\mathrm{T7}}}{K^{\mathrm{T5}}}}\left(V_{GS}^{\mathrm{T7}} - V_T^{\mathrm{T7}}\right) \right) \end{aligned} \tag{8}$$

$$b = -G_{ADC}\frac{n^{\mathrm{T1}}kT}{q} \tag{9}$$

$$c = \frac{I_S}{G_A G_L G_Q A} \tag{10}$$

$$\epsilon = \epsilon_Q + \epsilon_N + \epsilon_M. \tag{11}$$

III. Calibration and Correction

Since the complexity of calibration and correction depends on the number of parameters that vary spatially, no more variables should be permitted than are absolutely necessary. Sections III-A, III-B, and III-C consider the scenarios where (1) offset (or single) variation, (2) offset and gain (or double) variation, or (3) offset, gain and bias (or triple) variation causes FPN.

Analytic solutions are possible for single and double variation since correction, resulting in a logarithmic representation of the scene, is performed by a linear transform. For triple variation, parameters are estimated by iteration since correction, resulting in a linear representation of the scene, is performed by a nonlinear transform. In all cases, the residual error is assumed to be statistically independent from observation to observation and pixel to pixel and to follow a zero-mean Gaussian distribution. Such assumptions reduce maximum likelihood estimation of the model parameters to least squares estimation [8].

A. Offset Variation

Equation (12) estimates the response $\hat{y}_{ij}$ of the jth pixel, in an array of N pixels, to a stimulus x_i, when the offset a_j varies spatially. The gain b and bias c are constant for all pixels. Due to (7), the estimated response $\hat{y}_{ij}$ differs from the actual response y_{ij} by lacking an unpredictable error component ϵ_{ij}:

$$\hat{y}_{ij} = a_j + b\ln(c + x_i). \tag{12}$$

The model parameters may be estimated by minimizing the sum square error (SSE), defined in (13) below, between the actual response y_{ij} of the image sensor and the estimated response $\hat{y}_{ij}$ to M different but uniform stimuli x_i:

$$SSE = \sum_{i=1}^{M}\sum_{j=1}^{N}(y_{ij} - \hat{y}_{ij})^2. \tag{13}$$

The SSE does not have a unique global minimum because (12) is invariant under transformations (14)–(16), which means that all parameters cannot be estimated from the data y_{ij}:

$$(a_j, b, c, x_i) \equiv (a_j, b, c - \gamma, x_i + \gamma) \tag{14}$$

$$\equiv \left(a_j, \frac{b}{\gamma}, 0, (c + x_i)^{\gamma}\right) \tag{15}$$

$$\equiv (a_j - b\ln\gamma, b, \gamma c, \gamma x_i). \tag{16}$$

Intuitively, the offset of a pixel is proportional to the difference between the pixel's average response and the average response of all pixels, a method by which Loose *et al.* (among others) correct FPN [7]. Equation (17) gives the average response $\bar{y}_i$ of all pixels to illuminance x_i, which relates to the parameters by (18), with $\bar{a}$ in (19), since y_{ij} and $\hat{y}_{ij}$ differ by random variables ϵ_{ij} that are assumed to have zero mean:

$$\bar{y}_i = \frac{1}{N}\sum_{j=1}^{N} y_{ij} \tag{17}$$

$$\bar{y}_i \approx \bar{a} + b\ln(c + x_i) \tag{18}$$

$$\bar{a} = \frac{1}{N}\sum_{j=1}^{N} a_j. \tag{19}$$

Comparing (12) and (18), the estimated response $\hat{y}_{ij}$ may be written as a linear function, in (20), of the average response $\bar{y}_i$, with one variable a'_j, in (21), per pixel:

$$\hat{y}_{ij} = a'_j + \bar{y}_i \tag{20}$$

$$a'_j = a_j - \bar{a}. \tag{21}$$

The minimum of the SSE occurs when the partial derivatives, in (22), of the SSE with respect to the variables a'_j equal zero. Solving for a'_j at the minimum of the SSE gives estimates $\hat{a}_j$ in (23), where $\bar{y}_j$ and $\bar{y}$ in (24) and (25) are the average response of the j^{th} pixel and of all pixels respectively:

$$\frac{\partial SSE}{\partial a'_j} = -2\sum_{i=1}^{M}(y_{ij} - a'_j - \bar{y}_i) \tag{22}$$

$$\hat{a}_j = \bar{y}_j - \bar{y} \tag{23}$$

$$\bar{y}_j = \frac{1}{M}\sum_{i=1}^{M} y_{ij} \tag{24}$$

$$\bar{y} = \frac{1}{M}\sum_{i=1}^{M} \bar{y}_i. \tag{25}$$

Three variables $\bar{a}$, b and c remain unknown, consistent with (14)–(16). Nonetheless, single variation may be corrected for an image y_j by subtraction, as in (26), leaving an FPN-free estimate $\hat{y}_j$ related to the logarithm of the scene x_j and limited by the unpredictable residual error:

$$\hat{y}_j = y_j - \hat{a}_j \approx \bar{a} + b\ln(c + x_j). \tag{26}$$

The variance $\hat{\sigma}^2_{\epsilon}$ of the residual error is estimated in (27) from the calibration data y_{ij}. The variance equals the SSE in (13) divided by the degrees of freedom (DOF), which provides an unbiased estimate [9]. The DOF, given in (28), is the number of constraints MN (i.e., y_{ij}) minus the number of variables $M+N$ (i.e., $\bar{y}_i$ and $\hat{a}_j$) fitted to the same constraints:

$$\hat{\sigma}^2_{\epsilon} = \frac{1}{DOF}\sum_{i=1}^{M}\sum_{j=1}^{N}(y_{ij} - \hat{y}_{ij})^2 \tag{27}$$

$$DOF = MN - M - N. \tag{28}$$

Equation (29) estimates the variance $\hat{\sigma}_{\epsilon_i}$ of the residual error from pixel responses at the ith illuminance. Section IV uses this statistic to identify and characterize a dependence of error on illuminance, which violates the assumptions, if it exists:

$$\hat{\sigma}^2_{\epsilon_i} = \frac{M}{DOF}\sum_{j=1}^{N}(y_{ij} - \hat{y}_{ij})^2. \tag{29}$$

B. Offset and Gain Variation

Equation (30) estimates the response $\hat{y}_{ij}$ of the jth pixel, in an array of N pixels, to an illuminance x_i, when the offset a_j and gain b_j vary spatially. The bias c is constant for all pixels:

$$\hat{y}_{ij} = a_j + b_j \ln(c + x_i). \tag{30}$$

As before, the model parameters may be found by minimizing the SSE in (13). The SSE does not have a unique global minimum because (30) is invariant under transformations (14)–(16) (with b replaced by b_j). Intuitively, correcting the offset and gain variation should move the response of a pixel close to the average response of all pixels. This average $\bar{y}_i$ in (17) relates to the parameters by (31), with $\bar{a}$ and $\bar{b}$ in (19) and (32):

$$\bar{y}_i \approx \bar{a} + \bar{b} \ln(c + x_i) \tag{31}$$

$$\bar{b} = \frac{1}{N} \sum_{j=1}^{N} b_j. \tag{32}$$

Comparing (30) and (31), $\hat{y}_{ij}$ is a linear function, in (33), of $\bar{y}_i$, with two variables a'_j and b'_j, in (34) and (35), per pixel:

$$\hat{y}_{ij} = a'_j + b'_j \bar{y}_i \tag{33}$$

$$a'_j = a_j - b'_j \bar{a} \tag{34}$$

$$b'_j = \frac{b_j}{\bar{b}}. \tag{35}$$

Minimizing the SSE between y_{ij} and $\hat{y}_{ij}$ is similar to solving N independent linear regression problems where the abscissae are $\bar{y}_i$ and the ordinates are y_{ij}. Thus, a'_j and b'_j may be estimated by $\hat{a}_j$ and $\hat{b}_j$ in (36) and (37) using the equations of linear regression [9], where $\bar{y}_j$ and $\bar{y}$ are given in (24) and (25):

$$\hat{a}_j = \bar{y}_j - \hat{b}_j \bar{y} \tag{36}$$

$$\hat{b}_j = \frac{\sum_{i=1}^{M} (y_{ij} - \bar{y}_j)(\bar{y}_i - \bar{y})}{\sum_{i=1}^{M} (\bar{y}_i - \bar{y})^2}. \tag{37}$$

Three variables $\bar{a}$, $\bar{b}$ and c remain unknown, as in Section III-A. Nonetheless, double variation may be corrected for an image y_j by subtraction and division, as in (38), giving a result $\hat{y}_j$ that is proportional to the logarithm of the scene x_j:

$$\hat{y}_j = \frac{y_j - \hat{a}_j}{\hat{b}_j} \approx \bar{a} + \bar{b} \ln(c + x_j) \tag{38}$$

Equations (27) and (29) estimate the variance of the residual error using the DOF in (39) instead of (28), which accounts for the two fitted parameters per pixel:

$$DOF = MN - M - 2N. \tag{39}$$

C. Offset, Gain, and Bias Variation

Although it begins the same way, calibration of triple variation differs from that of single and double variation. Equation (40) estimates the response $\hat{y}_{ij}$ of the jth pixel, in an array of N pixels, to an illuminance x_i, where a_j, b_j, and c_j vary spatially:

$$\hat{y}_{ij} = a_j + b_j \ln(c_j + x_i). \tag{40}$$

The model parameters may be found by minimizing the SSE in (13). The SSE does not have a unique global minimum because (40) is invariant under transformations (14) and (16) (with b and c replaced by b_j and c_j), but (15) does not apply because of bias variation. Unlike before, the intuitive approach, i.e., fitting the response of each pixel to the average response, fails. Although the average $\bar{y}_i$ in (17) relates to the parameters by (41), with $\bar{a}$ in (19), $\hat{y}_{ij}$ cannot be written as a linear function of $\bar{y}_i$ because of the nonlinear effect of bias variation:

$$\bar{y}_i \approx \bar{a} + \frac{1}{N} \sum_{j=1}^{N} b_j \ln(c_j + x_i). \tag{41}$$

However, $\hat{y}_{ij}$ is a linear function, given in (42), of l_{ij}, defined in (43), but l_{ij} depends on the unknown bias and illuminance:

$$\hat{y}_{ij} = a_j + b_j l_{ij} \tag{42}$$

$$l_{ij} = \ln(c_j + x_i). \tag{43}$$

Assuming l_{ij} is known, minimizing the SSE between y_{ij} and $\hat{y}_{ij}$ is equivalent to solving N independent linear regression problems with abscissae l_{ij} and ordinates y_{ij}. Thus, a_j and b_j may be estimated by $\hat{a}_j$ and $\hat{b}_j$ in (44) and (45) using linear regression [9], with $\bar{y}_j$ and $\bar{l}_j$ in (24) and (46):

$$\hat{a}_j = \bar{y}_j - \hat{b}_j \bar{l}_j \tag{44}$$

$$\hat{b}_j = \frac{\sum_{i=1}^{M} (y_{ij} - \bar{y}_j)(l_{ij} - \bar{l}_j)}{\sum_{i=1}^{M} (l_{ij} - \bar{l}_j)^2} \tag{45}$$

$$\bar{l}_j = \frac{1}{M} \sum_{i=1}^{M} l_{ij}. \tag{46}$$

Equations (43)–(46) show that, at the minimum of the SSE, $\hat{a}_j$ and $\hat{b}_j$ are known functions of c_j and x_i. Therefore, the minimum SSE is a known function of only c_j and x_i, which reduces the number of variables by almost two-thirds. No analytic expression for c_j and x_i that minimizes the SSE has been found because the partial derivatives of the SSE with respect to c_j and x_i are highly nonlinear. However, the conjugate gradient algorithm [8] finds the minimum successfully by iteration.

Minimization yields estimates $\hat{c}_j$ and $\hat{x}_i$ within a linear transform of the actual biases c_j and illuminances x_i because of (14) and (16). Nonetheless, triple variation may be corrected for an image y_j by the nonlinear transform in (47), where $\hat{a}_j$ and $\hat{b}_j$ are found using (44) and (45). Unlike in sections Sections III-A and III-B, the FPN-free estimate $\hat{x}_j$ approximates a linear function of the scene x_j, with an unknown offset α and gain β (that depend on the normalization of conjugate gradient estimates $\hat{c}_j$ and $\hat{x}_i$):

$$\hat{x}_j = \exp\left(\frac{y_j - \hat{a}_j}{\hat{b}_j}\right) - \hat{c}_j \approx \alpha + \beta x_j. \tag{47}$$

Equations (27) and (29) estimate the variance of the residual error using the DOF in (48) instead of (28), which accounts for the three fitted parameters per pixel:

$$DOF = MN - M - 3N. \tag{48}$$

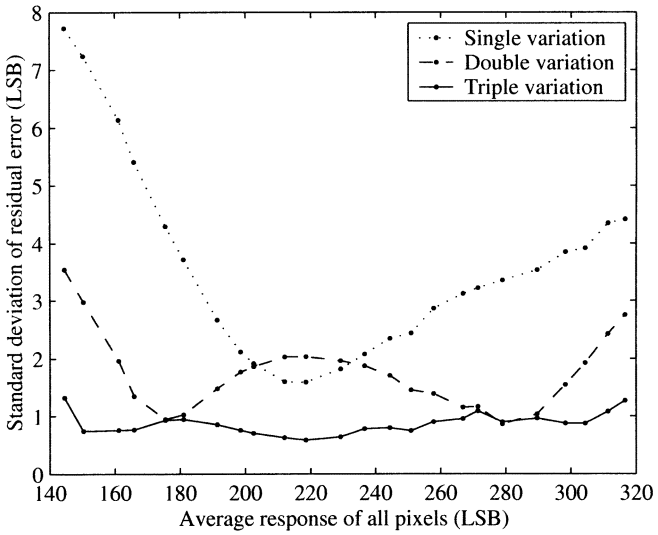

Fig. 2. Standard deviation $\hat{\sigma}_{\epsilon_i}$ of residual error versus average response $\bar{y}_i$ of all pixels for calibration of the single, double, and triple variation models.

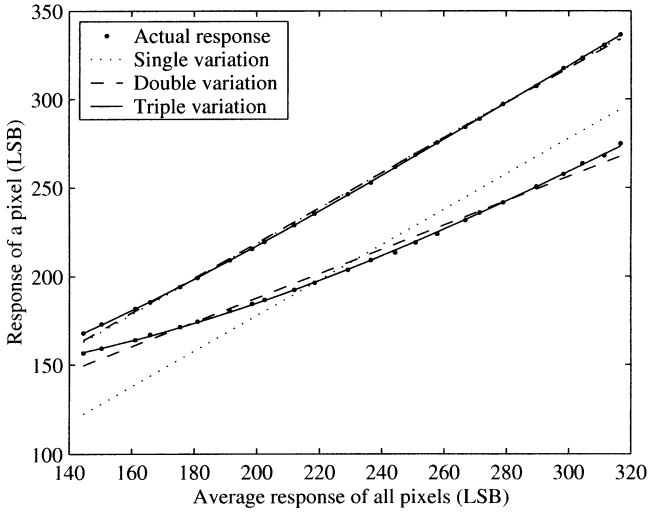

Fig. 3. Actual y_{ij} and estimated $\hat{y}_{ij}$ response of two pixels versus average response $\bar{y}_i$ of all pixels for the single, double, and triple variation models.

IV. Experimental Results

Experiments were done using a 512 by 512 pixel ($N = 512^2$) Fuga 15d logarithmic image sensor [4]. The camera, interfaced to a PC, had an 8-bit ADC with a programmable offset voltage F_{ADC}. By capturing several frames with different offset settings, the resolution was increased to 10 bits in software. Images of a white sheet of paper under uniform illumination provided calibration data y_{ij}. The iris ring was rotated, thereby changing the aperture, to vary the illumination reaching the focal plane. Parameters of the single, double and triple variation models were estimated according to Section III.

A. Calibration

The first experiment used an 800 W tungsten lamp, with a filter to simulate daylight and involved 24 images ($M = 24$) to permit a detailed comparison of results. After calibration, the standard deviation $\hat{\sigma}_\epsilon$ of the residual error was 3.9, 1.9, and 0.9 LSB for the single, double and triple variation models, which may not appear to be a significant difference. However, when the error is shown versus illuminance, as in Fig. 2, the models differ markedly. The single variation model has a minimum error of two LSB in the middle of the domain, with error rising on each side to eight and four LSB. The double variation model has a maximum error of two LSB in the middle, flanked by two minima of one LSB and rising to four and three LSB at the sides. In contrast, the triple variation model has a flat error of less than one LSB. The small but sharp rises at the sides may be due to parameter overfitting, which would favor the midrange of data. These results suggest that the nonlinear triple variation model fits the data very well, at least in the estimated dynamic range of three decades.

Fig. 3 shows the actual and estimated response of two pixels. While the single variation model fits the top pixel's response well, it does not fit the bottom pixel's response because of a different response slope from one pixel to the other. Instead, it intersects the response in the middle, minimizing the SSE, which explains the v-shaped curve in Fig. 2. The double variation model matches the response slopes of both pixels but intersects each response twice as the actual response follows a curved path (especially the bottom one). This accounts for the w-shaped curve in Fig. 2. For the bottom pixel's response, note that single variation near its intersection is better than double variation, which explains the small region of Fig. 2 where the former outperforms the latter. The triple variation model has no problem following the curved responses of both pixels and the residual error varies randomly with illuminance in Fig. 2.

B. Correction

Fig. 4 shows four scenes after FPN correction, using the single, double, and triple variation models (calibrated in fluorescent light with only five images of white paper, i.e., $M = 5$). The triple variation result was displayed on a logarithmic scale for consistency. The four scenes are really one scene made darker by changing the aperture from 1.8 (wide open) to 4, 8, and 16 f-stops. The inter-scene dynamic range is 38 dB and the intra-scene dynamic range is 29 dB, for a total of 67 dB.

Because the scenes are the same going from top to bottom in Fig. 4 except getting darker, an ideal logarithmic image sensor would give the same response with a progressively more negative offset. Since each image has been stretched linearly to fit the 8-bit range of the display, images in a column should look identical. Triple variation correction gives good results and is better than single or double variation correction. Similarly, double variation gives better results than single variation.

V. Conclusion

This paper has modeled the response y of a logarithmic CMOS pixel to illuminance x. The model has numerous physical parameters but can be abstracted by a logarithmic function $y = a + b\ln(c + x) + \epsilon$ with only three parameters—an offset a, gain b and bias c—and a residual error ϵ. A spatial variation of the parameters leads to fixed pattern noise (FPN). Although it is well known that threshold voltage variation,

Fig. 4. A scene, using single, double, and triple variation correction (left to right), imaged with apertures of 1.8, 4, 8, and 16 f-stops (top to bottom).

in the pixel and column source follower transistors, leads to FPN, the model shows other contributions to offset variation and highlights possible sources of gain and bias variation. Bias variation makes the FPN a nonlinear function of illuminance.

Using least squares estimation, equations to extract the model parameters from images of uniform illuminance were derived. Exact solutions were given for the case where gain and bias variations are ignored and the case where bias variation is ignored. No exact solution was possible for the case where all three parameters vary spatially, but the number of unknowns was reduced analytically by two-thirds. The remaining parameters were successfully obtained by numerical optimization.

Experimental results with a Fuga 15d image sensor validate the nonlinear model and demonstrate calibration and correction. Although the overall residual error for calibration of single, double, and triple variation does not differ by much, the error versus illuminance differs substantially. The single and double variation models have v-shaped and w-shaped error curves, proving they are inaccurate. In contrast, the triple variation model has an error less than one LSB and is independent of illumination over approximately three decades of intensity.

Whether nonlinear correction proves to be a practical approach to correct FPN in logarithmic CMOS image sensors remains to be seen. Nonetheless, while analog techniques to correct pixel and column offsets, such as double sampling and delta difference sampling, are useful to reduce FPN (and $1/f$ noise), they are inadequate for a logarithmic sensor operating over a high dynamic range. The same may be said for digital correction of offset variation or even offset and gain variation. The nonlinear effect of offset, gain and bias variation on FPN requires more robust circuits or nonlinear correction.

REFERENCES

[1] K. Diefendorff, "CMOS Image Sensors Challenge CCDs," *Microprocessor Rep.*, pp. 1–5, June 1998.

[2] S. K. Mendis, S. E. Kemeny, R. C. Gee, B. Pain, C. O. Staller, Q. Kim, and E. R. Fossum, "CMOS active pixel image sensors for highly integrated imaging systems," *IEEE J. Solid-State Circuits*, vol. 32, pp. 187–97, Feb. 1997.

[3] T. Zarnowski, T. Vogelsong, and J. Zarnowski, "Inexpensive image sensors challenge CCD supremacy," *Photon. Spectra*, pp. 188–92, May 2000.

[4] B. Dierickx, D. Scheffer, G. Meynants, W. Ogiers, and J. Vlummens, "Random addressable active pixel image sensors," in *Proc. SPIE*, vol. 2950, Oct. 1996, pp. 2–7.

[5] D. Scheffer, B. Dierickx, and G. Meynants, "Random addressable 2048 x 2048 active pixel image sensor," *IEEE Trans. Electron Devices*, vol. 44, pp. 1716–20, Oct. 1997.

[6] O. Yadid-Pecht, "Wide-dynamic-range sensors," *Opt. Eng.*, vol. 38, no. 10, pp. 1650–60, Oct. 1999.

[7] M. Loose, K. Meier, and J. Schemmel, "CMOS image sensor with logarithmic response and self-calibrating fixed pattern noise correction," in *Proc. SPIE*, vol. 3410, May 1998, pp. 117–27.

[8] C. M. Bishop, *Neural Networks for Pattern Recognition*. Oxford, U.K.: Oxford Univ. Press, 1995.

[9] R. L. Scheaffer and J. T. McClave, *Probability and Statistics for Engineers*. Belmont, CA: Wadsworth, 1995.

Dileepan Joseph received the B.Sc. degree in computer engineering in 1997 from the University of Manitoba, Winnipeg, MB, Canada. He received the D.Phil. degree in engineering science from the University of Oxford, Oxford, U.K., under a fellowship from the Natural Sciences and Engineering Research Council of Canada. His doctoral research concerned logarithmic CMOS image sensors.

Mr. Joseph was a recipient of the University Gold Medal in Engineering, University of Manitoba, and the Governor General's Silver Medal.

Steve Collins received the B.Sc. degree in theoretical physics from the University of York, York, U.K., in 1982 and the Ph.D. degree from the University of Warwick, Warwick, U.K., in 1986.

From 1985 to 1997, he worked at the Defence Research Agency on various topics including the origins of 1/*f* noise in MOSFETs and analog information processing. Since 1997, he has been with the University of Oxford, Oxford, U.K., where he has continued his interest in smart imaging sensors and nonvolatile analog memories.